Densification Leveraging Mobility

An IoT Architecture Based on Mesh Networking and Vehicles

Chang-Sik Choi
The University of Texas at Austin
Austin, Texas
chang-sik.choi@utexas.edu

François Baccelli
The University of Texas at Austin
Austin, Texas
baccelli@math.utexas.edu

Gustavo de Veciana
The University of Texas at Austin
Austin, Texas
gustavo@ece.utexas.edu

ABSTRACT

Disruptive changes are underway in the automotive industry as large-scale platforms based on vehicular fleets are deployed to deliver ride sharing and delivery services. Such platforms can also be leveraged to deliver wireless connectivity services, e.g., large-scale connectivity for the Internet of Things (IoT). This paper examines a network architecture based on a mesh of IoT devices, roadside repositories and vehicular mobile gateways – referred to as mesh+vehicular. We propose a system-level model to study its relative merits versus conventional infrastructure-based IoT architectures– referred to as mesh+cellular. The model reflects the salient properties of the architectures including the key interplay among the variability in the network geometries, routing trees, wireless capacity and eventually IoT queue stability.

The paper provides an initial study of the scaling of the IoT *sensing capacity* of the routing trees per repository and base station respectively for the two architectures: i.e., the scaling the maximum common traffic rate the trees' IoT devices can generate while maintaining the stability of its queues. We then define the *harvesting capacity* per mobile gateway and base station in the two architectures, i.e., the average aggregate IoT rate each can extract assuming IoT devices are limited to their sensing capacity in each tree. Perhaps surprisingly, we show that as the spatial density λ_s of IoT devices and corresponding density of repositories along roads scale up, the proposed mesh+vehicular architecture has a gain in its harvesting capacity of order at least $\lambda_s^{\gamma/4}$ where γ is the wireless path loss exponent. Underlying such gains is a fundamental shift in network geometry and information flows: in mesh+cellular systems IoT data is routed toward cells' sinks (zero-dimensional objects) while in mesh+vehicular data is routed to road induced cell edges (one-dimensional objects). Detailed system-level simulations validate the obtained scaling results.

CCS CONCEPTS

• **Networks → Wireless mesh networks**; *Network architectures*; *Network performance analysis*; *Network structure*;

KEYWORDS

Internet-of-Things, Radial spanning trees, Queuing theory, Kelly networks, Network capacity

ACM Reference Format:
Chang-Sik Choi, François Baccelli, and Gustavo de Veciana. 2018. Densification Leveraging Mobility: An IoT Architecture Based on Mesh Networking and Vehicles. In *Mobihoc '18: The Eighteenth ACM International Symposium on Mobile Ad Hoc Networking and Computing, June 26–29, 2018, Los Angeles, CA, USA.* ACM, New York, NY, USA, 10 pages. https://doi.org/10.1145/3209582.3209590

Mobihoc '18, June 26–29, 2018, Los Angeles, CA, USA

ACM ISBN 978-1-4503-5770-8/18/06…$15.00
https://doi.org/10.1145/3209582.3209590

1 INTRODUCTION

1.1 Motivation

The automotive industry is undergoing disruptive changes. In particular, the emergence of large-scale platforms for ride sharing and delivery services is expected to result in fleets of shared driverless transportation vehicles. Such fleets deliver compelling capital and operational cost reductions through substantially improved resource utilization possibly disrupting the traditional paradigm of vehicle ownership [30]. Further, by freeing people from driving, it is expected that the personalization and customization of vehicle riders' experience will be critical, including the opportunities to enhance productivity and/or entertainment while in motion. To that end, vehicles will need to be extremely well connected to the infrastructure. In the context of such changes, we revisit a complementary question: how can a fleet of well-connected vehicles be leveraged to enable new forms of connectivity? In particular, how could such fleets be used to provide new forms of large-scale connectivity for IoT?

1.2 Background and Related Work

The IoT serves as a platform to interconnect sensor/tag/device nodes which facilitate monitoring of physical processes, tracking entities, and capturing information. Such networks are expected to become part of the fabric of modern life, supporting a wide range of applications in smart cities as well as agricultural and ecological applications in rural areas. According to Cisco's VNI technical report [15], by 2020, the density of IoT devices could reach $10^5/\text{km}^2$ in urban to suburban areas. In order to provide connectivity to such high numbers of heterogeneous IoT devices, diverse technologies are envisioned, from RFID, Bluetooth, Zigbee, and standard Wifi, to emerging standards such as low power Wifi, low-power-wide-area (LPWA), and Narrowband IoT (NB-IoT) [4]. To enable Internet connectivity for IoT devices with limited power, short transmission range, and possibly sporadic traffic. mesh based relaying has been proposed. Indeed architectures using multi-hop relaying towards

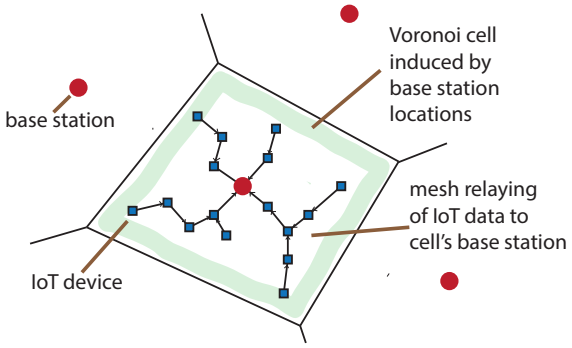

Figure 1: mesh+cellular architecture where IoT traffic is relayed to the base station at the Voronoi center.

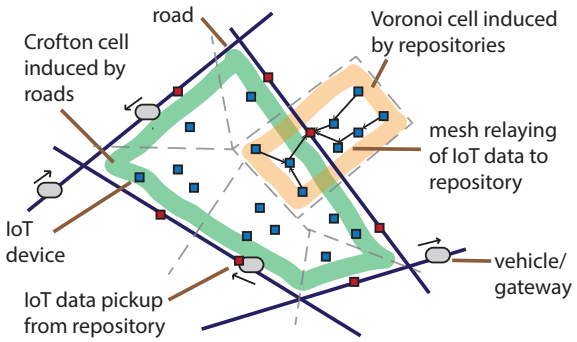

Figure 2: Illustration of the vehicular+mesh architecture that relay IoT traffic to repositories at the cell edges. The IoT traffic is relayed to its nearest repository.

sinks connected to the Internet have been studied since the early 2000s [1, 6, 32]. and [31] for example product. We refer to these a *mesh+cellular* architectures, see Figure 1.

In this paper, we consider an alternative which leverages mesh networking and vehicular fleets – we refer to this as *mesh+vehicular*, see Figure 2. In this architecture, IoT devices forward their uplink data towards repositories (possibly simply IoT devices or dedicated road side units) at the nearest road using multi-hop relaying. Vehicles serve as Internet gateways which opportunistically pick up data from repositories next to roads.

Such architectures are not new, indeed they fall in the class of Delay Tolerant Networks (DTN). DTNs have been extensively studied in, e.g., [2, 21, 22, 28]. A seminal paper in this area is [21], where it was first shown that mobility could significantly increase the capacity of networks if one could tolerate delays. Subsequently, DTNs with mobile nodes received substantial attention, see e.g., [11, 24, 29]. The scaling properties of DTNs were studied in a series of key papers including [19, 21]. The trade-off relationship between delay and throughput was specifically analyzed in [20]. Most of the theoretical work on DTNs has focused on networks with a single type of node: typically, a human carrying a mobile phone, or vehicles [10, 33]. The key novelty of the study in this paper is that it incorporates the geometry and dynamics of the network elements: (1) vehicles move along and repositories are located on roads (2) IoT devices are randomly scattered in space inducing flows on radial spanning trees. To our knowledge, there has been no system-level study of the capacity of such architectures.

The challenge in developing such an analysis is the mix of random geometric structures (cells, routing trees, roads), wireless capacity (interference, SIR, Shannon rate), and dynamics (relaying, queuing, vehicular pickup). This paper uses stochastic geometry to model the geometric structures and information and queuing theory to compare the capacity scaling of mesh+cellular and the mesh+vehicular architectures. The geometric structures for both the are random objects in the Euclidean plane. We also make the use of Palm calculus [8] which allows one to define the characteristics of typical objects (typical cell, typical mesh tree, etc.) in such networks. Our analysis is based on Poisson assumptions (Poisson line process and Poisson point processes) which have been used extensively in the study of cellular wireless networks in [5, 8, 16] while the Poisson line Cox model was leveraged to model vehicular networks in [13, 27]. The dynamic aspects associated with vehicular pickup have not been previously studied in these works.

1.3 Contributions

The primary contributions of this paper are as follows.

(1) *Network model combining large-scale geometry and dynamics with small-scale wireless characteristics.* We propose an develop a simple model capturing the salient features of mesh+vehicular (and mesh+cellular) architectures. The model includes elements of the *large-scale* geometry such as the road system where vehicles and repositories move/lie and routing of IoT devices' traffic along induced spatial trees. The model also captures *small-scale* characteristics, such as the signal-to-interference ratio (SIR) of wireless links on trees, which are linked via Shannon's capacity formula to the service rates for IoT relaying queues in the routing trees. Overall, to our knowledge this is the first attempt to capture and study the characteristics and interplay of geometry and variability at different scales.

(2) *Study of network performance and capacity gain.* We provide definitions for the sensing capacity and harvesting capacity of the network architectures and characterize their scaling properties as the density of IoT devices λ_s (and associated repositories) increases. The *sensing capacity* is defined as the maximal common sensing rate that IoT devices sharing a routing tree to a repository/base station can generate while maintaining the stability of the IoT queues in trees. We then define *harvesting capacity* per mobile gateway and base station in the two architectures, i.e., the average aggregate IoT rate each can extract assuming IoT devices are limited to the sensing capacity in each tree. Perhaps surprisingly, we show that the gain in the harvesting capacity of mesh+vehicular over mesh+cellular architecture is of order $\lambda_s^{\gamma/4}$ where γ models the wireless channel path loss. This establishes the enormous potential that a shift from routing traffic inwards to sinks (as in cellular-based networks) to routing traffic outwards to cell edges (i.e., repositories on roads as in vehicular networks) would provide. Our analysis further highlights the complex interplay between large-scale geometry (e.g., change in IoT traffic flows) and small-scale fluctuations (e.g.,.due to local variations in interference) play in limiting capacity. In particular,

we highlight the key role of the theory of extremes of small-scale fluctuations, in determining the sensing capacity bottlenecks. Complementary detailed simulation results validate the scaling gain results.

2 SYSTEM MODEL

This section describes the spatial model, the relaying strategy, the queuing models, performance metrics, and preliminary results. Before introducing our spatial model, we remind the reader that the Voronoi tessellation induced by the realization of a point process $\Phi = \{x_i \in \mathbb{R}^2, i \in \mathbb{N}\}$ is defined by $V_\Phi = \{V_\Phi(x_i), x_i \in \Phi\}$ where $V_\Phi(x_i) = \{x \in \mathbb{R}^2 \,|\, \|x - x_i\| \leq \|x - x_j\|, j \neq i\}$ is the Voronoi cell associated with $x_i \in \Phi$. For instance, if Φ is a Poisson point process, V_Φ is the Poisson-Voronoi tessellation.

2.1 Spatial Model

2.1.1 Mesh+cellular architecture. We model the locations of base stations for the mesh+cellular architecture by a planar Poisson point process (PPP) Φ_b with density λ_b. In addition, we model the locations of IoT devices as an independent planar PPP Φ_s with intensity λ_s. Each base station is assumed to serve uplink traffic of IoT devices in its Voronoi cell. Figure 1 illustrates the mesh+cellular architecture. Note that the cellular architecture in this paper captures the traditional infrastructure-based architectures, e.g., could be either cellular or wifi, but without mobile gateways.

2.1.2 Mesh+vehicular architecture. As briefly discussed in Introduction, in the proposed mesh+vehicular architecture, vehicles play the role of gateways. Since vehicles travel on roads, we model the network of roads as a stationary Poisson line process (PLP) Φ_l represented by a PPP Ξ on the cylinder set $\mathbf{C} = \mathbb{R} \times [0, \pi]$. Specifically, each point of Ξ, say (r, θ), corresponds to a line in the Euclidean space specified by $\{(x, y) \in \mathbb{R}^2 \,|\, x \cos\theta + y \sin\theta = r\}$, where r denotes the distance from the origin to the line and θ denotes the angle between the positive $x-$axis and the unit normal vector to the line, measured in the counterclockwise direction. The intensity measure of Ξ is given by $\Lambda_\Xi(\mathrm{d}r\,\mathrm{d}\theta) = \lambda_l\,\mathrm{d}r G(\mathrm{d}\theta) = \frac{\lambda_l}{\pi}\,\mathrm{d}r\,\mathrm{d}\theta$. Note that we consider $G(\mathrm{d}\theta) = \frac{\mathrm{d}\theta}{\pi}$, then the PLP yields randomly displaced lines (see Fig. 3 top). If the intensity measure along θ-axis is concentrated, $G(\mathrm{d}\theta) = \frac{1}{2}\delta_0 + \frac{1}{2}\delta_{\pi/2}$, the PLP Φ_l yields only vertical and horizontal lines, which is referred to as a Manhattan line process (see Fig. 3 bottom). The lines on the plane tessellate the Euclidean space into the Crofton cells.

Conditionally on the PLP Φ_l, vehicles are distributed according to a stationary PPP Ψ_v with intensity μ_v on each line. Collectively, those PPPs form what is referred to as a Poisson line Cox point process, $\Phi_v = \{\Psi_v\}$. Note that the distance between the two closest points on the same line follows an exponential distribution with parameter μ_r and PPPs on different lines are conditionally independent. We assume, for simplicity, that each vehicle moves at a constant speed v along its road, choosing its direction with probability 1/2.

Similarly, conditionally on the same realization of the PLP, repositories are modeled via a PPP Ψ_r with intensity μ_r on each line. Hence, collectively, the PPPs $\{\Psi_r\}$ form a Poisson line Cox point process denoted by $\Phi_r = \{\Psi_r\}$. Notice that the PPPs for vehicles and repositories $\{\Psi_v, \Psi_r\}$ are conditionally independent. Figure 3 illustrates the Poisson line Cox point process and its Voronoi cells.

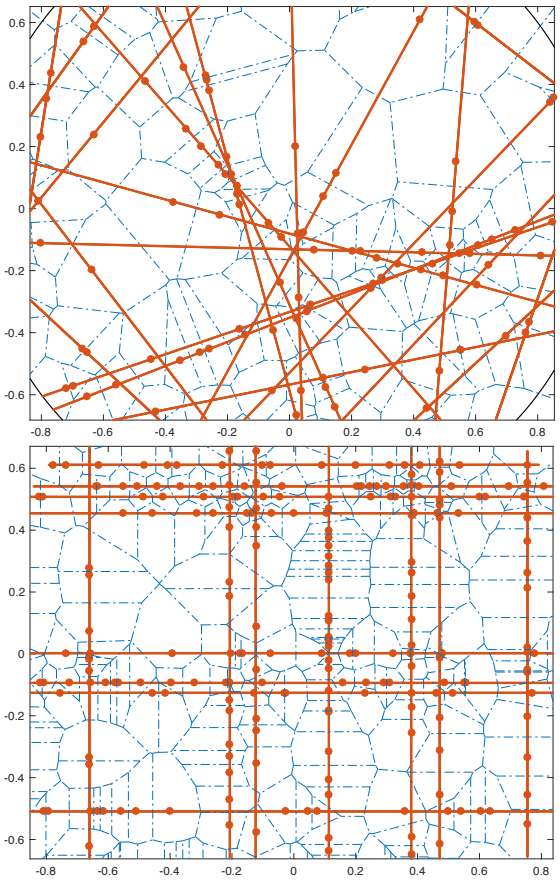

Figure 3: Illustration of the Poisson line Cox point process (circles), PLP (solid lines), and the Voronoi cells (dashed lines) where $G(\mathrm{d}\theta) = 1/\pi\,\mathrm{d}\theta$ or $G(\mathrm{d}\theta) = 0.5\delta_0 + 0.5\delta_{\pi/2}$, respectively.

As for the mesh+cellular architecture, the locations of the IoT devices in the mesh+vehicular architecture are modeled by an independent planar PPP Φ_s with intensity λ_s. Figure 2 illustrates all the elements of the mesh+vehicular architecture.

2.2 Stochastic Geometry and Typicality

Palm calculus allows one to define typicality. For instance, under the Palm distribution of Φ_r, one sees the typical Cox-Voronoi cell, or equivalently the Voronoi cell of a typical repository. Intuitively, the typical Cox-Voronoi cell is one of the two-dimensional objects surrounded by the dashed lines in Fig. 3, selected at random. Similarly, under the Palm probability of Φ_b, one sees the typical Poisson-Voronoi cell. The typical Cox-Voronoi and Poisson-Voronoi cells are random polygons. Their geometric properties, such as the lengths of edges, angles between edges, and areas, are characterized by their probability distributions. Nevertheless, even for the simplest case, which is that of the typical Voronoi cell of a homogeneous PPP, the distribution of the area of the cell is still unknown. Analyzing

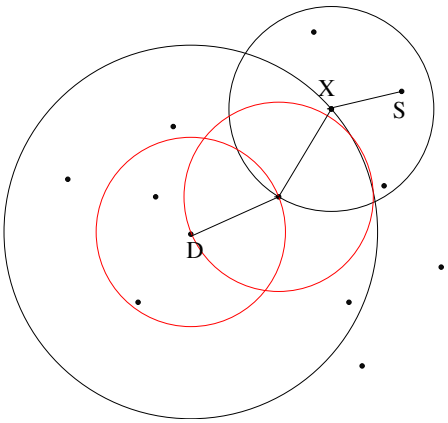

Figure 4: Path of the radial spanning tree from source S to destination S. For the destination D, the next hop from device X is chosen among the devices closer to D than X. The next hop is the device which is the closest to X.

the distribution of the typical cell is hence out of the scope of this paper. The only results available on these random objects regard their moments, e.g., mean area. Here is a summary of the results on first order moments for typical cells that will be used below.

Lemma 1. *In the mesh+vehicular architecture, the densities of repositories is $\mu_r\lambda_l$ and the mean area of the typical repository Voronoi cell is given by $(\mu_r\lambda_l)^{-1}$. In the mesh+cellular architecture, the density of base stations is λ_b and the mean area of the typical base station Voronoi cell is ${\lambda_b}^{-1}$.*

For the proof of above, the mesh+vehicular architecture is discusssed in [14] and the mesh+cellular architecture is discussed in [12].

2.3 Mesh Networking and Routing

This paper considers a tractable nearest neighbor routing strategy. The source forwards its traffic (packet) to its nearest relay that is closer to its destination than itself (and to the destination directly if there is no such relay). The associated paths are mathematically characterized by *radial spanning trees*[1] [9] on the mesh of IoT devices. Figure 4 illustrates the radial spanning tree from source S to destination D. Specifically, in both architectures, IoT devices are sources and relays at the same time. Base stations and repositories are destinations in the mesh+cellular architecture and the mesh+vehicular architecture, respectively. Based on the geometry, IoT devices decide their destinations to be their closest base station in the mesh+cellular architecture or their closest repository in the mesh+vehicular architecture, respectively.

In the mesh+vehicular architecture, IoT devices follow the strategy explained above, and therefore IoT meshes are characterized by

[1]Suppose two IoT nodes X, Y in $\mathcal{V}$ the Voronoi cell centered at the origin. Then, there exists a directed edge of radial spanning tree rooted at the origin if

$$\|Y-O\| < \|X-O\| \text{ and } \Phi_s(\mathcal{V}\cap B_O(\|X\|)\cap B_Y\|X-Y\|) = \emptyset,$$

where $B_x(r)$ denotes the ball of radius r centered at $x \in \mathbb{R}^2$. In other words, X has an edge toward Y if Y is closer to the root and there exists no other IoT device at the intersection of the Voronoi cell $\mathcal{V}$, the ball centered at the origin with radius $\|X\|$, and the ball centered at the X with radius $\|X-Y\|$.

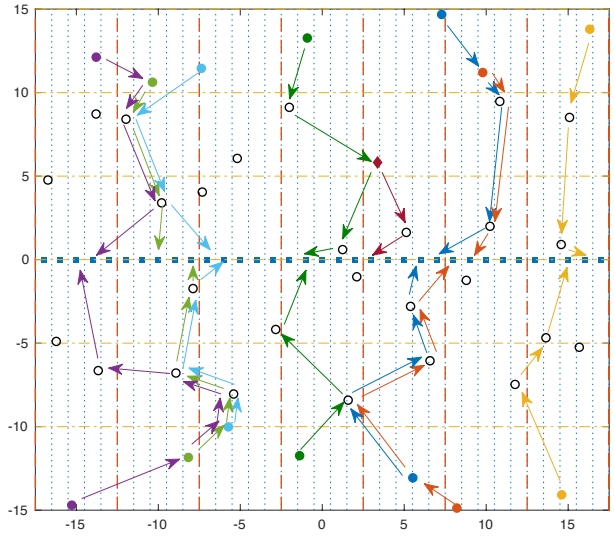

Figure 5: Simplified example of relaying from IoT nodes to repositories. Filled disks illustrate sources, blue squares and dotted lines describe repository (Cox point process) and the Cox-Voronoi cells.

radial spanning trees on IoT devices rooted at repositories. Recall that, contrarily to the base stations in the mesh+cellular architecture, repositories hold IoT data until it is delivered to a vehicle passing by. Consequently, the mesh+vehicular architecture involves two types of packet transmissions: wireless multi-hop relaying of IoT devices to the repositories, and wireless transmissions from repositories to vehicles.

2.4 Congestion Model

As mentioned in the introduction, the traffic in our two architectures will experience congestion in distinctive ways, e.g, around zero dimension base station sinks or around one dimension cell edges. To capture these characteristics we introduce the simplest queuing model as follows.

2.4.1 Queuing model for IoT Mesh. Each IoT device $x_i \in \varphi_s$ is assumed to generate sensing data packets according to a Poisson process with intensity ξ packets/sec and packets are assumed to have exponentially distributed size with mean $1/\alpha$ bits. In addition to its own traffic each IoT device may serve as a relay to other node's traffic. Thus each IoT queue may carry traffic from several upstream nodes as a result of radial spanning tree routing to repositories/base stations. Note that an IoT node may relay IoT packets heading to different destinations/next hops and thus different service rates.

Consequently, under the radial spanning routing of IoT traffic, the overall network can be viewed as a multi-class Kelly network where packets associated with different radial spanning trees correspond to different classes (see e.g. [25]). See Figure 5 for the illustration of the Kelly network in simplified geometry where for simplicity repositories are equally spaced. Specifically, all packets in the same class are relayed to their corresponding relay sharing the same exponential packet service time. The packet service rate

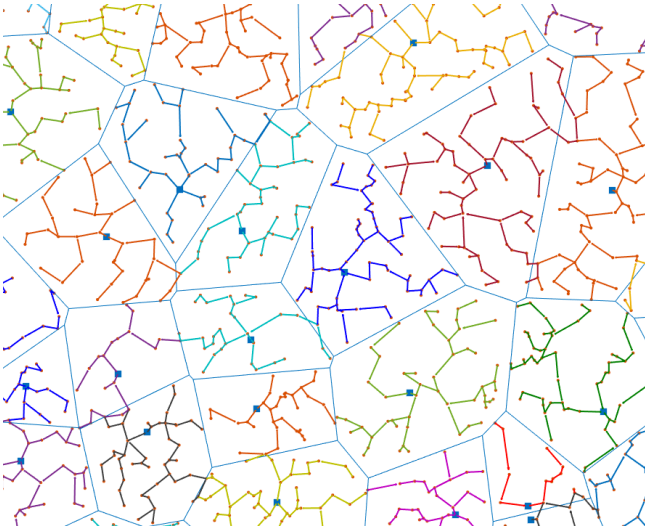

Figure 6: Different classes are in different colors.

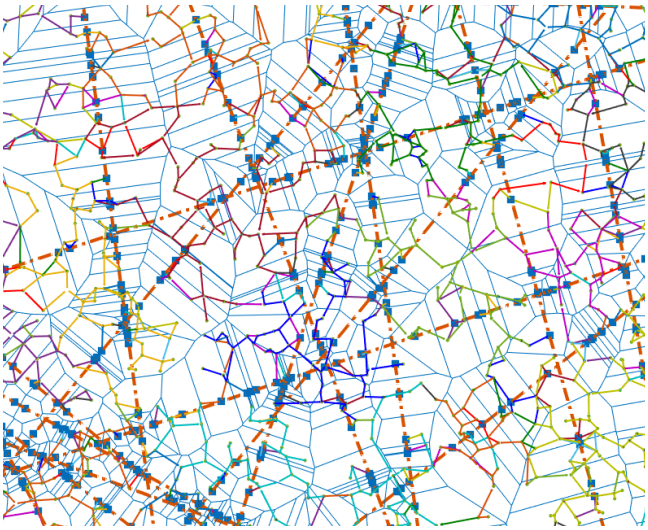

Figure 7: Different classes are in different colors. The radial spanning graphs are coupled in space compared to the ones in Figure 6.

depends on the packet size and the associated wireless links' physical transmission rate which we will describe shortly. Note that all IoT devices in this paper are assumed to receive and transmit at the same time. Figures 6 and 7 illustrate the simulated topologies of the Kelly networks in both architectures.

2.4.2 Queuing model for repositories. In the mesh+vehicular architecture, repositories can only communicate *opportunistically* when vehicles pass by; thus, their characteristics are not well captured by an M/M/1 queuing model. A natural approach is to assume the repository queue (server) is active when one (or more) vehicles are in its Voronoi cell; otherwise, it shuts down (goes on vacation), until a new vehicle enters its cell. Such systems are referred to as queues with vacations, see e.g. [17], and can be somewhat complex to work with (see time-limited gated queues with vacations in e.g. [26]). In the spirit of the simplified models, we introduce an appropriate repository queuing model. Noticing that the inter-arrival times of vehicles can be interpreted as server vacations, we assume vehicles (servers) arrive to serve a repository queue as a Poisson process with rate $\mu_v v$. The inter-arrival time of vehicles is exponentially distributed with mean $(\mu_v v)^{-1}$ since the density of vehicles on the road is μ and their speed is v.

2.5 Wireless Link Capacity and Queue Service Rates

The service rate of each queue can be interpreted as the achievable transmission rate at its intended receiver. Without fading, the received signal power is assumed to be attenuated according to a general distance-based path loss model $\delta^{-\gamma}$ where δ is the distance and γ is the path loss exponent. Notice that the power law assumption on the path loss model underlies the main claims of this paper.

Without loss of generality, the bandwidth is assumed to be 1. Then, the transmission link rate $r_{i,j}$ from IoT node i to IoT node j is modeled by the Shannon rate formula based on signal-to-interference-ratio (SIR) and it is given by

$$r_{i,j} = \log_2(1 + \mathrm{SIR}_{i,j}) = \log_2\left(1 + \frac{\delta_{i,j}^{-\gamma}}{\sigma_j^2}\right), \tag{1}$$

where σ_j^2 is the interference at node j and $\delta_{i,j}$ is the distance from node i to its next hop node j. There is no difficulty in introducing fading in these formulas and in the subsequent analysis. Recall that IoT devices are assumed to receive and transmit concurrently.

Incorporating the transmission rate with the queuing model in the previous section, we get that the service rate ifor packets at IoT queue i which are relayed to j is given by $\eta_{i,j} = \alpha r_{i,j}$.

Similarly, the service rate of a repository queue to a vehicle v inside its Cox-Voronoi cell is given by $\eta_{r,v} = \alpha r_{r,v}$, where the transmission rate of repository node r to vehicle v is given by

$$r_{r,v} = \log_2\left(1 + \frac{\delta_{r,v}^{-\gamma}}{\sigma_v^2}\right) \tag{2}$$

where $\delta_{r,v}$ is the distance from repository r to vehicle v and σ_v^2 is the interference currently seen at vehicle v.

2.6 Performance Metrics

We will introduce two performance metrics to compare our network architectures: the sensing capacity and harvesting capacity. The first is formally introduced in this subsection while the second is relegated to Section 4.3

Consider a routing tree $\mathcal{T}_x$ associated with a base station sink or repository x. The tree includes all paths from IoT nodes in Voronoi cell of x to the sink/repository x. Each IoT device $i \in \mathcal{T}_x$ relays traffic on behalf of IoT nodes associated with destination x as well as possibly traffic on behalf of other destinations. Let H_i denote set of next hop nodes for routes traversing node i, and $\eta_{i,j}$ the link rate from IoT node i to j. Finally let $N_{i,j}$ denote the number of IoT nodes whose traffic is relayed by node i to next hop j including

possibly traffic generated by node i. Suppose each IoT device were to generate the same rate ξ then the mean load at node i denoted $\rho_i(\xi)$ is given by

$$\rho_i(\xi) = \sum_{j \in H_i} \frac{\xi N_{i,j}}{\eta_{i,j}} = \xi \sum_{j \in H_i} \frac{N_{i,j}}{\eta_{i,j}}. \quad (3)$$

Note that to ensure the stability of all the nodes in the tree one must ensure $\rho_i(\xi) < 1$ for all $i \in \mathcal{T}_x$. We shall define sensing capacity of the tree as the max rate ξ that satisfies such stability constraints.

Definition 1. *The IoT device sensing capacity of tree $\mathcal{T}_x$ is given by*

$$\xi_x := \min_{i \in \mathcal{T}_x} \frac{1}{\rho_i(1)}$$

Note in defining the sensing capacity of the tree $\mathcal{T}_x$, we assumed that all IoT nodes both associated with repository/base station x as well as others generate the *same* rate ξ. It is possible that traffic heading to other destinations may be bottlenecked elsewhere, which would allow the tree $\mathcal{T}_x$ to possibly render a higher minimum rate to its own IoT nodes. Thus the above characterization is in fact a lower bound on the minimum *common* rate that the tree can support, for its IoT devices.

Note also that due to the stochastic variations in tree size and overlaps as well as link rates each tree may achieve a different sensing capacity. In the sequel we will however study its scaling properties for a high-density regime.

3 SCALING OF NETWORKS

This section is focused on the basic geometrical properties of the spatial elements of the proposed models. In the asymptotic regime that we describe below, we fix every system parameter (including v, λ_l and μ_v), except for the spatial density of IoT devices λ_s and the linear density of repositories μ_r. Below, the notation $A \sim B$ indicates that A and B are of the same order, as $\lambda_s \to \infty$, i.e.,

$$0 < \liminf_{\lambda_s \to \infty} \frac{A}{B} \leq \limsup_{\lambda_s \to \infty} \frac{A}{B} < \infty.$$

For instance, if a function of λ_s is of order 1, it becomes a constant (up to a multiplicative constant) as λ_s tends to infinity.

3.1 Scaling of IoT Density

Assumption 1. *We consider a scaling where the density of IoT devices λ_s tends to ∞. In the mesh+cellular architecture, the density of base station is fixed. In the mesh+vehicular architecture, the density of roads and vehicles are fixed, but the density of repositories is assumed to satisfy*

$$\mu_r \sim \lambda_s.$$

Remark 1. *The comparison that we will make between the proposed mesh+vehicular architecture (where the density of repositories tends to infinity) and the mesh+cellular architecture (where the density of base stations is fixed) may look unfair due to the Assumption 1. In fact it is not. First, in the mesh+vehicular architecture, repositories are nothing but IoT devices located along roads. In other words, except for the fact that the repositories are on roads, their transmission range, buffer size, battery capacity, and cost are the same as those of IoT devices. Therefore, assuming a dense deployment of repositories is not restrictive in the context of a dense IoT setting. Second and more importantly, the analogue of base stations in the mesh+cellular setting is vehicles in the mesh+vehicular case. Both have the densities of order 1.*

Under the assumption, the distribution of the Cox-Voronoi cell can be further characterized as follows.

Lemma 2. *Under Assumption 1, the typical Cox-Voronoi cell w.r.t. Φ_r converges to a one-dimensional segment S almost surely in the Fell topology. Its length is given by the summation of two independent exponential random variables each with parameter $2\lambda_l$.*

See [14] for the proof.

4 MAIN CLAIMS

The main claims of this paper are given in the statement below. We note at the outset, that given the complexity of the systems under consideration we have resorted to rough mathematical *scaling analysis* that will require formal proofs, however, all of the results have been validated via simulation. Thus we shall refer to our results as "claims" and provide rough "proofs" based on expected scaling properties. In this section, each IoT device packet size has the mean size of 1.

Claim 1. *Under Assumption 1 and for path loss exponent $\gamma \geq 2$, the mesh+vehicular architecture has a sensing capacity at least of order $\lambda_s^{-\gamma/4-1/2}$ and the mesh+cellular architecture has a sensing capacity of order $\lambda_s^{-\gamma/2-1/2}$.*

We shall informally establish this claim based on considering the large-scale network characteristics which are close to their means, radial spanning trees of IoT devices in these large-scale geometries, and local fluctuations in the wireless service rates and traffic in these trees which determine the order of the load at bottleneck queues.

4.1 Mesh+Vehicular Sensing Capacity

Let C_x denote the Cox-Voronoi cell of repository at x and $\Phi_s(C_x)$ the set of IoT nodes located inside C_x. Then, the collection of all paths starting from a node in $\Phi_s(C_x)$ to root x forms a tree which is denoted by $\mathcal{T}_x$. Further, we shall let $\mathcal{V}_x$ denote the set of vertices of $\mathcal{T}_x$. It is important to note that in general, although the root x and its leaves $\Phi_s(C_x)$ are in the Cox-Voronoi cell C_x, most vertices of $\mathcal{T}_x$ are outside of C_x particularly when the Cox-Voronoi cells are very thin – see Figures 5 and 7.

Claim 2. *Under Assumption 1 the cardinality of the set $\mathcal{V}_x$ is of order $\sqrt{\lambda_s}$.*

Proof. The typical Cox-Voronoi cell C_x has an area of order $1/\lambda_s$ since its width has order $1/\lambda_s$ and its height has order 1 – see Lemma 3. So the cardinality of $\Phi_s(C_x)$ is order 1. In our asymptotic regime, the length of each hop along the radial spanning tree towards the repository e.g., from $y \in \Phi_s(C_x)$ to x is of order $1/\sqrt{\lambda_s}$ [9]. Hence, the number of hops along such a path is order $\sqrt{\lambda_s}$ and since there is order 1 leaves in $\Phi_s(C_x)$, the cardinality of the set $\mathcal{V}_x$ is of order $\sqrt{\lambda_s}$. □

Let d be an IoT device. It may have several next hop nodes depending on the number of radial spanning trees, i.e., classes of packets, that contain it. Let H_d denote the set of next hop nodes for d. It is easy to check that the cardinality of H_d is of order 1. Consider now the queue of device d. In this queue, the service time of a packet with next hop $h \in H_d$ is an exponential random variable with parameter

$$\log_2\left(1+\frac{S(d,h)}{I(h)}\right),$$

where $S(d,h)$ is the receive power at h from d, namely $\|h-d\|^{-\gamma}$, and $I(h)$ is the interference power at h. Recall packets are assumed to be exponentially distributed with mean 1, hence modeling the transmission rate by the Shannon capacity we obtain the above packet service rate.

Claim 3. *Under Assumption 1, the largest mean packet service time b_x in the tree $\mathcal{T}_x$ is of order $\lambda_s^{\gamma/4}$.*

Proof. By approximating $\log(1+x)$ as x for $x \ll 1$, the largest mean service time experienced by a packet traversing nodes in (but not necessarily following) the tree $\mathcal{T}_x$ is given by

$$b_x = \max_{n\in\mathcal{V}_x}\max_{h\in H_n}\frac{I(h)}{S(n,h)}.$$

In the high density regime being considered, the rescaled shot noise $\frac{I(h)}{\lambda_s^2}$ converges in distribution to an alpha stable random variable $A(h)$ with parameter $2/\gamma$ [7]. Similarly, the ratio $\frac{\lambda_s^2}{S(n,h)}$ converges to a random variable $B(n,h)$ with a tail distribution function $\overline{F}(x)=\exp(-\pi x^{2/\gamma})$ (Weibull) truncated at λ_s^2 [23]. Hence, for some given λ_s, we have

$$\frac{I(h)}{S(n,h)} = A(h)\min(B(n,h),\lambda_s^2).$$

For a given h, the random variable $A(h)$ is large when there is an interfering transmitter close to h; whereas $B(n,h)$ is large when the distance between n and h is large. These extreme events are essentially independent. Therefore, using Breiman's lemma [18], the tail of the product $A(h)B(n,h)$ is given by a constant times that of $A(h)$.

Furthermore, the maximum of k independent alpha-stable random variables with parameter $2/\gamma$ is known to grow as $k^{\frac{\gamma}{2}}$ [7]. Since the tails of the random variables $A(h)B(n,h)$ are the same, up to multiplicative constant, as those of $A(h)$, and since these random variables are mixing w.r.t. h, it follows that the largest mean service time b_x in tree $\mathcal{T}_x$ is of order the maximum of $\sqrt{\lambda_s}$ (Claim 1) independent with the same distribution as $A(h)$, i..e, of order growing as $\lambda_s^{\gamma/4}$. □

For any IoT node y we shall let U_y denote the set of trees which contain y.

Claim 4. *Under Assumption 1 the cardinality of U_y of a typical IoT node y is of order $\sqrt{\lambda_s}$.*

Proof. Consider trees $\{\mathcal{T}_{x_i}\}$, where $\ldots, x_{-2}, x_{-1}, x_0, x_1, x_2, \ldots$ are successive repositories along a typical road. Note that these trees have common nodes and edges. By Claim 2 each tree has order $\sqrt{\lambda_s}$ nodes. So per unit length of road, the sum of the cardinalities of the trees is of order $\lambda_s\sqrt{\lambda_s}$. Since there are only λ_s nodes per unit of length, a typical node must belong to order $\sqrt{\lambda_s}$ trees. □

Recall that each Cox-Voronoi cell contains order 1 nodes ($\lambda_s \sim \lambda_l$), so each tree generates an overall traffic which is order 1. Hence, by Claim 4 above, it follows that the traffic through a typical IoT node is of order $\sqrt{\lambda_s}$.

Claim 5. *The sensing capacity of the mesh+vehicular architecture is at least of order $\lambda_s^{-\gamma/4-1/2}$.*

Proof. Let us first consider possible bottlenecks at IoT queues and then focus on repository nodes. There are two underlying reasons an IoT queue might become a bottleneck. First the service time to the next hop node of one of its packet classes (i.e., radial spanning trees that traverse it) could be huge. This could be due to a high interference or a poor signal. Recall the worst mean packet service time in a typical tree was evaluated in Claim 3 and is of order $\lambda_s^{\frac{\gamma}{4}}$. Second, the traffic (arrival rate) to the device is huge. These two phenomena are essentially independent. Due to the homogeneity of the IoT device locations, a service rate bottleneck is roughly equally likely to arise anywhere in a tree; a bottleneck arising at an IoT node serving packets with extremely high mean service times will thus see a traffic load given by arrival rate $\sqrt{\lambda}$ to a typical IoT node times the scaling of the worst case mean service time $\lambda_s^{\frac{\gamma}{4}}$ i.e., $\lambda_s^{\frac{\gamma}{4}+\frac{1}{2}}$ which is greater than λ_s for $\gamma \geq 2$. By contrast, a bottleneck arising at a node due to a huge traffic arrival rate, i.e., due to a large number of overlapping radial spanning trees sharing the node, will scale by no more than $\sqrt{\lambda_s}$ (Figure 8). This leads to the conclusion that the first type of IoT bottleneck, i.e., associated with a deviation in the mean service rates, dominates the second types associated with excessive packet arrivals rate. From this, a lower bound on the sensing capacity can be derived; if the bottlenecks indeed arise at IoT queues, then the scaling of the sensing capacity of the tree in the mesh+vehicular networks would be inversely proportional to the load i.e., at least of order $\lambda_s^{-\gamma/4-1/2}$.

On the other hand, for repository r, the traffic is of order 1 IoT nodes times the arrival rate each IoT queue in the tree. Moreover, using the cycle analysis in vacation queue [17], the service rate is $\frac{\frac{1}{\mu_r}}{\frac{1}{\mu_r}+\frac{1}{\mu_v}}\log_2\left(1+\frac{\delta_{r,v}^{-\gamma}}{\sigma_v^2}\right)$. Therefore, the bottleneck of a repository is given by

$$\frac{1}{\frac{\frac{1}{\mu_r}}{\frac{1}{\mu_r}+\frac{1}{\mu_v}}\log_2\left(1+\frac{\delta_{r,v}^{-\gamma}}{\sigma_v^2}\right)} \sim \frac{\lambda_s}{\log_2\left(1+\frac{\lambda_s^{\gamma}}{\lambda_s^{\gamma/2}}\right)} \sim \frac{\lambda_s}{\log_2(\lambda_s)}, \quad (4)$$

where we use the fact that under Assumption 1, $\delta_{r,v}$ is of order λ_s^{-1} since the scale of the width of the repository cell is of order λ_s^{-1} while the scale of $\sigma_{r,v}^2$ is of order $\lambda_s^{\gamma/2}$ [7] since a vehicle sees IoT interferers (density of order λ_s) and repository interferers (density of order 1) and IoT interferers dominate. Consequently, in the tree the IoT bottleneck dominates the repository bottleneck as $\lambda_s^{-\gamma/4-1/2} < \lambda_s/\log_2(\lambda_s)$, and thus the sensing capacity of mesh+vehicular architecture is of order $\lambda_s^{-\gamma/4-1/2}$ at least. □

4.2 Mesh+Cellular Sensing Capacity

Let P_x denote the Poisson-Voronoi cell of base station x and $\Phi_s(P_x)$ denote the set of IoT nodes in P_x. The collection of all paths starting from nodes $\Phi_s(P_x)$ and leading to x form a tree $\mathcal{T}'_x$. Let $\mathcal{V}'_x$ denote the vertices of $\mathcal{T}'_x$.

Claim 6. *Under Assumption 1 the cardinality of the set $\mathcal{V}'_x$ is of order λ_s.*

The following claim is similar to Claim 3 given in the previous subsection.

Claim 7. *Under Assumption 1 and if $\gamma \geq 2$ the largest mean service time for nodes in the tree $\mathcal{T}'_x$ is of order $\lambda_s^{\gamma/2}$.*

Claim 8. *Let y be the typical IoT device with associated base station x. The cardinality of the set of nodes in the subtree $\mathcal{T}_{x,y}$ made of nodes that use y as a relay their packets to x, is of order $\sqrt{\lambda_s}$. By contrast, nodes that are not typical, but instead known to be close to the base station x see traffic which is at most of order λ_s.*

Proof. The first property follows from unimodularity [3]. Pick a node y at random in the tree. Make this node the root in a random directed graph. This rooted graph is unimodular by construction. Send mass 1 from every node every other node downstream. The mean mass arriving at the root is the mean cardinality of the $\mathcal{V}_y$. The mean mass leaving the root is the length of the path from y to the base station. The latter has order $\sqrt{\lambda_s}$. This concludes the proof. □

Claim 9. *Under Assumption 1 and if $\gamma > 2$, the sensing capacity of the mesh+cellular architecture is of order $\lambda_s^{-\gamma/2-1/2}$.*

Proof. The argument is similar to that of Claim 5 in the previous subsection. The worst bottleneck arises either at a typical IoT node with extremely poor mean service rate or at a node seeing a particularly large traffic, i.e., nodes close to the base station. By Claim 8, the worst case mean service time of a typical node associated with a base station scales as $\lambda_s^{\gamma/2}$ and it in turn by Claim 8 will see an arrival rate from upstream nodes which is of order $\sqrt{\lambda_s}$, giving a total load $\lambda_s^{\gamma/2+1/2}$. Nodes close to the base station may see higher loads, i.e., order at most λ_s but the scaling of their service rate is much better than that of the IoT seeing the worst mean service. Hence, the capacity of the mesh+cellular architecture is of order $\lambda_s^{-\gamma/2-1/2}$. □

4.3 Comparison of Harvesting Capacities

The main merit of the mesh+vehicular architecture is that it allows one to connect a dense set of devices (density of order λ_s) to a sparse set of gateways namely base stations or mobile gateways (density of order 1) using thin mesh trees (vertices of order $\sqrt{\lambda_s}$). In contrast, the mesh+cellular architecture involves fat ball-shaped trees (with a number of vertices of order λ_s).

The first advantage of these thinner trees is that they have less severe wireless bottlenecks, i.e., service times, compared to those of the larger trees in the mesh+cellular architecture, as stressed in Claims 3 and 7 above. It should be stressed that the main reasons for the gain are (1) trees used in the mesh+vehicular architecture have less nodes in average than those used in the mesh+cellular architecture and (2) the metric (worst bottleneck) is computed per tree. The worst wireless bottleneck in a collection of order λ_s thin trees of the vehicular setting (with a total number of devices order λ_s) would be the same as in the ball-shaped tree of the cellular case.

Since trees have so different in their sizes, a fair comparison would be made by taking the viewpoint of a typical gateway vs. a typical base station, rather than by taking a typical repositry vs. a typical base station. This requires the introduction of a new metric, harvesting capacity.

Definition 2. *The harvesting capacity of a gateway (base station sink or vehicle) is defined by the mean number of packets (or equivalently bits $\alpha = 1$) that the gateway receives per unit of time assuming that each tree operates just below its sensing capacity.*

Finally, the fair comparison of the architectures should be made by comparing the harvesting capacity of gateways in each architecture. The following claim is the main claim of this paper.

Claim 10. *A harvesting capacity gain of order at least $\lambda_s^{\gamma/4}$ exists when moving from the cellular architecture to the vehicular architecture.*

Proof. Over a time interval of length l, a base station harvests order $\lambda_s^{-\gamma/2+1/2}$ packets because there are order λ_s sensing flows and each flow has order $\lambda_s^{-\gamma/2-1/2}$. During the same time interval, a vehicular gateway visits $vl\lambda_s$ repositories. The mean number of packets it harvests per repository is at least of order $\lambda_s^{-\gamma/4-1/2}$. By multiplying them[2] the vehicular gateway harvests at least of order $vl\lambda_s^{-\gamma/4+1/2}$ packets. For comparison of orders, consider $v = l = 1$. □

5 SIMULATION RESULTS

This section presents simulation methodology and results. The system level simulator is meticulously designed in order to conform to the models proposed in Section 2. In particular, for the mesh+cellular architecture, both the Poisson point process for base stations and the Poisson point process for IoT devices are simulated. Based on the deployment of the Poisson base stations and IoTs, the destination of each IoT device is determined based on the Voronoi tessellation. Given the geometry of point processes and corresponding Voronoi tessellation, radial spanning trees for mesh networking lead to multi-class routing networks (Figure 6). Then, from each IoT queue, different Shannon rates are derived for different classes and they are exactly determined by using the interference seen by the node and next hop distances. Then, using the stability condition of multi-class queues Eq. (3), the sensing capacity is derived.

In the same vein, for the mesh+vehicular architecture, the Poisson point process for IoT devices and the Cox point processes for repositories are simulated. Based on the layout of IoTs, roads, repositories, and Cox-Voronoi tessellation, the radial spanning trees are simulated to define the multi-class routing networks. (Figure 7). Similar to the mesh+cellular case, the sensing capacity of each tree is found by identifying the worst queue in the tree. Notice that the

[2] Note that we implicitly used a spatial ergodic theorem when summing up the numbers of packets harvested in the sequence of repository trees visited by the vehicular gateway. This ergodic theorem is justified by the mixing properties of the model and by the fact that sensing capacity is locally defined.

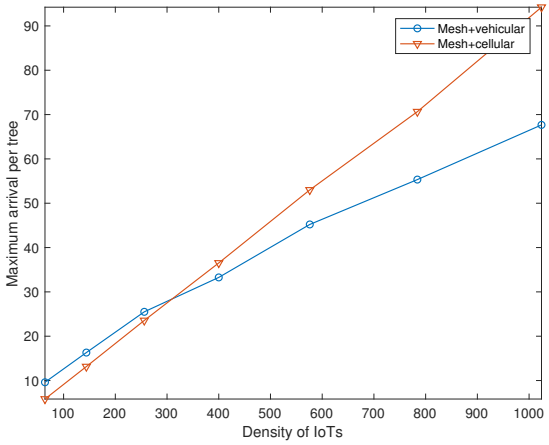

Figure 8: Maximum traffic among nodes per tree.

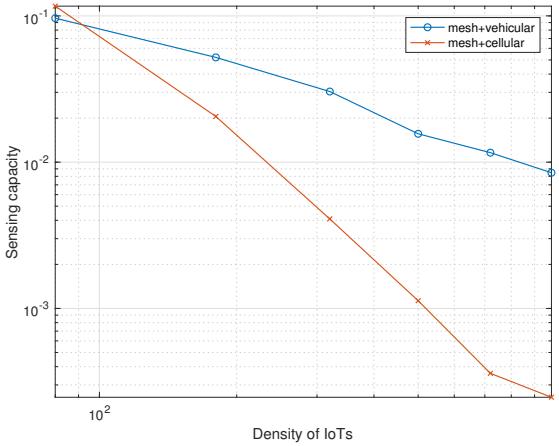

Figure 9: Sensing capacity. This is a loglog plot. Slopes are -1 and -2.5.

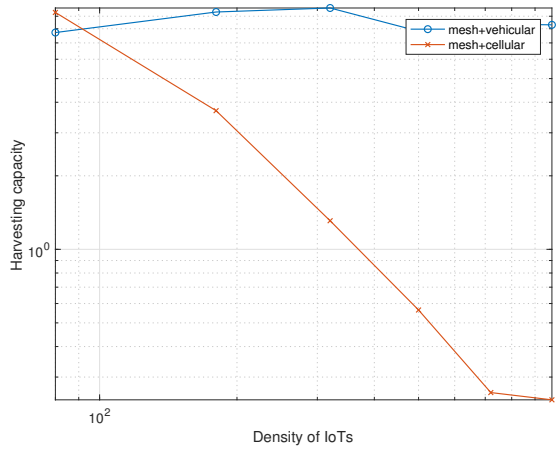

Figure 10: Harvesting capacity. This is a loglog plot. Slopes are 0 and -1.5.

queues in the mesh+vehicular architecture are two types: repository and IoT queues. The service rate of the repository queue is derived from the geometry, namely the width of the Cox-Voronoi cell. By identifying the minimum queue in each tree and spatially averaging the capacities of trees, the sensing capacity of the mesh+vehicular architecture is derived.

To obtain simulation results, we consider a network in a disk of radius 1km where the density of base stations is $\lambda_b = 10/\text{km}^2$ and the density of roads is $\lambda_l = 1/\text{km}$. The density of IoT devices varies in order to test the network capacity in dense regimes; specifically, $\lambda_s = 4\lambda_l\mu_r$. We consider the path loss exponent $\gamma = 4$.

5.1 Maximum Traffic

Figure 8 plots the maximum traffic (packet arrival toward IoT devices) per tree, i.e., $\mathcal{T}_x$ and $\mathcal{T}'_x$, obtained by simulation, in the mesh+vehicular and mesh+cellular architectures, respectively. As the density of IoT devices increases, the worst traffic is of order $\sqrt{\lambda_s}$ in the mesh+vehicular architecture. On the other hand, as the density increases, the worst traffic is of order λ_s in the mesh+cellular architecture.

5.2 Sensing Capacity and Harvesting Capacity

Figure 9 plots the sensing capacities and Figure 10 plots the harvesting capacities obtained by simulations. From the obtained graphs, the sensing capacity of mesh+vehicular architecture is of order λ_s^{-1} that is greater than the lower bound identified in Claim 5 and that of mesh+cellular architecture is of order $\lambda_s^{-2.5}$ as presented in Claim 9. The harvesting capacity of vehicular is given by of orders 1 that is greater the lower bound in the proof of Claim 10. The harvesting capacity of cellulra is given by of order $\lambda_s^{-1.5}$ as presented in Claim 10. The harvesting gain is of order 1.5 and it is greater than the lower bound in Claim 10

6 CONCLUSION AND FUTURE WORK

The results in this paper characterize the potential gains that densification leveraging mobility on road-based vehicular networks could bring. In particular the IoT architecture based on repositories and mobile gateways enables a shift from routing flows inwards to zero-dimensional sinks to routing traffic outwards towards one-dimensional cell edges, which should not only improve capacity but also distribute the congestion/energy burdens across the network. The mesh+vehicular architectures route traffic along thinner mesh trees towards repositories, experiencing less severe traffic and wireless capacity bottlenecks vs those in the larger trees of the conventional mesh+cellular architecture.

This work is only a very first step in this direction. Several complementary directions should be investigated.

A first important question that we leave for future work is whether the capacity gain brought by the mesh+vehicular architecture is robust to changes in the wireless path loss models, e.g., bounded ones. Indeed our analysis relies on the extremal properties

of the local interference, which play a dominant role in dictating the location and scaling of the queueing bottlenecks on sensing capacity. These are in turn depend fundamentally on the path loss model.

Second, since the dominant bottleneck so far has been driven by interference, another natural question is what would be the effect on scaling of introducing physical layer or protocol based techniques to mitigate interference. For instance, rather than treating interference as noise, one could use interference cancellation and mitigate strong interferers. This could, in principle, remove service time (wireless link capacity) fluctuations so that all link service times are order 1. Hypothetically this would leave fluctuations in the traffic loads across the trees as the determining factor for the sensing and harvesting capacities. From the claims of Section 4, we get that the mesh+cellular architecture has the worst traffic bottleneck of order $1/\lambda_s$ (at the nodes close to the base station) whereas the worst bottleneck of the mesh+vehicular architecture is the repository, and is of order $\log(\lambda_s)/\lambda_s$. Thus we might hope the gain is still present but logarithmic rather than polynomial in λ_s.

Finally, the results presented in this paper are based on arguments mixing mathematical claims validated via simulation which are still far from rigorous proofs. Our future work is geared at creating needed foundations to allow more rigorous analysis for both power-law and more general path loss models.

REFERENCES

[1] Abbasi, A. A., and Younis, M. A survey on clustering algorithms for wireless sensor networks. *Computer Commun. 30*, 14 (2007), 2826–2841.

[2] Akyildiz, I. F., Wang, X., and Wang, W. Wireless mesh networks: a survey. *Computer networks 47*, 4 (2005), 445–487.

[3] Aldous, D., Lyons, R., et al. Processes on unimodular random networks. *Electronic Journal of Probability 12* (2007), 1454–1508.

[4] Andreev, S., Galinina, O., Pyattaev, A., Gerasimenko, M., Tirronen, T., Torsner, J., Sachs, J., Dohler, M., and Koucheryavy, Y. Understanding the IoT connectivity landscape: a contemporary M2M radio technology roadmap. *IEEE Commun. Mag. 53*, 9 (2015), 32–40.

[5] Andrews, J. G., Baccelli, F., and Ganti, R. K. A tractable approach to coverage and rate in cellular networks. *IEEE Trans. Commun. 59*, 11 (2011), 3122–3134.

[6] Atzori, L., Iera, A., and Morabito, G. The internet of things: A survey. *Computer Networks 54*, 15 (2010), 2787–2805.

[7] Baccelli, F., and Biswas, A. On scaling limits of power law shot-noise fields. *Stochastic Models 31*, 2 (2015), 187–207.

[8] Baccelli, F., Błaszczyszyn, B., et al. Stochastic geometry and wireless networks: Volume ii applications. *Foundations and Trends® in Networking 4*, 1–2 (2010), 1–312.

[9] Baccelli, F., and Bordenave, C. The radial spanning tree of a Poisson point process. *The Annals of Applied Probability* (2007), 305–359.

[10] Benamar, N., Singh, K. D., Benamar, M., El Ouadghiri, D., and Bonnin, J.-M. Routing protocols in vehicular delay tolerant networks: A comprehensive survey. *Computer Communications 48* (2014), 141–158.

[11] Chaintreau, A., Hui, P., Crowcroft, J., Diot, C., Gass, R., and Scott, J. Impact of human mobility on opportunistic forwarding algorithms. *IEEE Trans. Mobile Comput. 6*, 6 (2007).

[12] Chiu, S. N., Stoyan, D., Kendall, W. S., and Mecke, J. *Stochastic geometry and its applications*. John Wiley & Sons, 2013.

[13] Choi, C.-S., and Baccelli, F. An analytical framework for coverage in cellular networks leveraging vehicles. *arXiv preprint arXiv:1711.09453* (2017).

[14] Choi, C.-S., and Baccelli, F. Poisson cox point processes for vehicular networks. *arXiv preprint arXiv:1801.04556* (2018).

[15] Cisco. Cisco visual networking index: Forecast and methodology 2014–2019 white paper. *Cisco, Tech. Rep* (2015).

[16] Dhillon, H. S., Ganti, R. K., Baccelli, F., and Andrews, J. G. Modeling and analysis of k-tier downlink heterogeneous cellular networks. *IEEE J. Sel. Areas Commun. 30*, 3 (2012), 550–560.

[17] Doshi, B. T. Queueing systems with vacations—a survey. *Queueing systems 1*, 1 (1986), 29–66.

[18] Embrechts, P., Klüppelberg, C., and Mikosch, T. *Modelling extremal events: for insurance and finance*, vol. 33. Springer Science & Business Media, 2013.

[19] Franceschetti, M., Dousse, O., David, N., and Thiran, P. Closing the gap in the capacity of wireless networks via percolation theory. *IEEE Trans. Inf. Theory 53*, 3 (2007), 1009–1018.

[20] Gamal, A. E., Mammen, J., Prabhakar, B., and Shah, D. Throughput-delay trade-off in wireless networks. In *Proc. IEEE INFOCOM* (2004), vol. 1.

[21] Grossglauser, M., and Tse, D. Mobility increases the capacity of ad-hoc wireless networks. In *Proc. IEEE INFOCOM* (2001), vol. 3, pp. 1360–1369.

[22] Gupta, P., and Kumar, P. R. The capacity of wireless networks. *IEEE Trans. Inf. Theory 46*, 2 (2000), 388–404.

[23] Haenggi, M. On distances in uniformly random networks. *IEEE Trans. Inf. Theory 51*, 10 (Oct 2005), 3584–3586.

[24] Hui, P., Crowcroft, J., and Yoneki, E. Bubble rap: Social-based forwarding in delay-tolerant networks. *IEEE Trans. Mobile Comput. 10*, 11 (2011), 1576–1589.

[25] Kelly, F. P. *Reversibility and stochastic networks*. Cambridge University Press, 2011.

[26] Leung, K. K., and Eisenberg, M. A single-server queue with vacations and gated time-limited service. *IEEE Trans. Commun. 38*, 9 (1990), 1454–1462.

[27] Morlot, F. A population model based on a poisson line tessellation. In *Proc. IEEE WiOpt* (2012), pp. 337–342.

[28] Ozgur, A., Lévêque, O., and David, N. Hierarchical cooperation achieves optimal capacity scaling in ad hoc networks. *IEEE Trans. Inf. Theory 53*, 10 (2007), 3549–3572.

[29] Spyropoulos, T., Psounis, K., and Raghavendra, C. S. Spray and wait: an efficient routing scheme for intermittently connected mobile networks. In *Proc. ACM SIGCOMM workshop on Delay-tolerant networking* (2005), pp. 252–259.

[30] Stocker, A., and Shaheen, S. Shared automated vehicles: Review of business models. In *International Transport Forum* (2017).

[31] Veniam: An Internet of Moving Things. http://veniam.com. Accessed: 2017-12-01.

[32] Zemlianov, A., and de Veciana, G. Capacity of ad hoc wireless networks with infrastructure support. *IEEE J. Sel. Areas Commun. 23*, 3 (2005), 657–667.

[33] Zeng, Y., Xiang, K., Li, D., and Vasilakos, A. V. Directional routing and scheduling for green vehicular delay tolerant networks. *Wireless Networks 19*, 2 (2013), 161–173.